Journal of Applied Physics

Atomistic simulations of tungsten nanotubes under uniform tensile loading

Cite as: J. Appl. Phys. **126**, 095105 (2019); https://doi.org/10.1063/1.5110167
Submitted: 14 May 2019 . Accepted: 12 August 2019 . Published Online: 03 September 2019

Travis Trusty, Shuozhi Xu, and Irene J. Beyerlein

AIP Publishing

Journal of Applied Physics ARTICLE scitation.org/journal/jap

Atomistic simulations of tungsten nanotubes under uniform tensile loading

Cite as: J. Appl. Phys. **126**, 095105 (2019); doi: 10.1063/1.5110167
Submitted: 14 May 2019 · Accepted: 12 August 2019 ·
Published Online: 3 September 2019

Travis Trusty,[1,a)] Shuozhi Xu,[2] and Irene J. Beyerlein[3]

AFFILIATIONS

[1]Department of Mechanical Engineering, University of California, Santa Barbara, Santa Barbara, California 93106-5070, USA
[2]California NanoSystems Institute, University of California, Santa Barbara, Santa Barbara, California 93106-6105, USA
[3]Materials Department and Department of Mechanical Engineering, University of California, Santa Barbara, Santa Barbara, California 93106, USA

[a)]**Author to whom correspondence should be addressed:** ttrusty@ucsb.edu

ABSTRACT

Metallic nanotubes (NTs) have gained much attention in recent years due to their exciting potential to be just as strong or even stronger than their heavier counterparts, nanowires (NWs), with the same outer radius. Unlike NWs, NTs have inner wall diameter and wall thickness parameters that can be engineered to provide advantage in structural materials design. In this work, molecular dynamics is used to quantify the combined effects of NT specific dimensions, outer radius and wall thickness, on the tensile strength of single crystalline tungsten NTs at room temperature. Uniaxial tensile simulations are carried out for three different crystallographic orientations along the NT axis—two known as brittle orientations and one as ductile orientation. For these three orientations, the strength of NTs can be made higher than NWs, for the same outer radius, as the wall thickness decreases. The calculations indicate that even for the brittle orientations, NTs can be engineered to be more ductile by tuning the outer radius and the wall thickness.

https://doi.org/10.1063/1.5110167

I. INTRODUCTION

Metallic nanowires (NWs) are widely employed in electronic and medical devices[1,2] due to their characteristically small volume and high strength (as compared with their bulk counterparts).[3] They are 1D materials with an axial dimension that is much larger than those within the cross-sectional plane.[4,5] NWs have been used to increase the absorption efficiency in solar cells, deliver drugs across the cell membrane, and add strength to (while reducing the weight of) structural materials.[6] Nanotubes (NTs) are hollow NWs that introduce an interior, concentric wall along the central axis. They can provide a promising alternative to NWs because NTs are lighter and can be stronger than NWs.[7] Moreover, NT wall thickness t serves as an additional geometric parameter that can potentially augment its properties compared to those of NWs with the same outer radius R.

Of interest here are the size effects of the NT wall thickness on mechanical properties. In face-centered cubic (FCC) Au NWs, most gliding dislocations may be absorbed by the free outer surfaces, resulting in a "dislocation starvation" state whose further plastic deformation requires an increase in the external loading.[8] Compared to NWs, NTs have a larger free surface area due to the inner wall, which can potentially result in a higher rate of dislocation starvation and a higher yield stress. Quantifying the effects of NT t has been most often studied via molecular dynamics (MD) simulations. Cao *et al.*[7] found that certain wall thicknesses t and lattice orientations enable ultrahigh strength and plasticity in Au NTs. Sun *et al.*[9] documented yield strength gains of up to 60% in Au NTs compared to Au NWs of a similar size. Amorim *et al.*[10] observed that Au and Cu NTs can sustain larger forces than NWs prior to structural rearrangement and rupture. Ji and Park[11,12] demonstrated that the elastic and mechanical properties of Cu NTs strongly depended on their geometric properties, such as the amount of materials removed from the central region of Cu NWs and the overall area of the NTs. Wang *et al.*[13] showed in Ni NTs that, with the same wall thickness t, Young's modulus increases with a decreasing outer radius R. Rojas-Nunez *et al.*[14] revealed that, compared with polycrystalline Ni NWs, polycrystalline Ni NTs have the same Young's modulus and ultimate tensile stress, as well as a higher fracture strain.

Most studies on NTs focused on those made from FCC crystals, such as Au,[7,9,10] Cu,[10–12] and Ni.[13,14] Far fewer atomistic simulations have been performed on NTs made of body center cubic (BCC) metals. In Ref. 15, the tensile deformation of W ⟨112⟩-oriented NTs with an outer radius of 20 nm was simulated. The NTs exhibited a lower strength than their NW counterparts regardless of the wall thickness t. Thus, it seems that reductions in weight offered by NTs are accompanied by sacrifices in strength. Yet, the sensitivity of strength to t seen in this one study only calls for more studies on the size effects in structural BCC NTs.

There are many reasons to expect that the mechanical behavior of NTs made from BCC metals may differ from those made from the more commonly studied FCC metals. Compared with their FCC counterparts, BCC metals have a larger number of slip systems.[16] It is also known that in BCC metals, due to low dislocation mobility of screw-oriented dislocations, the dislocation starvation state is less likely to occur.[8] Recent MD simulations have suggested that these differences in dislocation processes can have impact on the NT response, particularly in the failure mode. Using atomistic simulation, Xu *et al.*[17–19] found that W NWs consistently demonstrated a weaker size dependence in yield strength than FCC NWs. In studies of ⟨112⟩-oriented NTs in Ref. 15, it was found that t played a significant role in this transition. When $t > 2$ nm, NTs deformed in a ductile manner and their strengths are nearly independent of t, whereas when $t \leq 2$ nm, NTs failed in a brittle manner and the strengths decreased with smaller t. Atomistic simulations in nanotwinned NWs found that, when the twin boundary spacing reduces to about 3 nm, a brittle-to-ductile and a ductile-to-brittle transition is observed in FCC Cu[20] and FCC Au,[21] respectively, while no transition is found in either nanotwinned BCC Fe[22] or nanotwinned BCC W,[23] which remain ductile.

In this paper, we carry out MD simulations to model uniaxial tensile deformation of NTs in pure BCC W at room temperature of 300 K. Bulk W single crystals and W NWs are also studied for comparison. The effects of the crystallographic orientation, the wall thickness, and the outer radius on the ductile-to-brittle response and underlying deformation mechanisms are investigated. The calculations indicate that NTs can outperform NWs with similar R in yield and ultimate strength, and specific stiffness. We identify a critical volume-to-surface-area ratio V:S at which peak strength is achieved. These findings contribute to the understanding of size effects on the strength of NWs and NTs made of W and W alloys.[24]

II. METHODS

The simulation cells of the W bulk single crystals and W NTs are illustrated in Fig. 1. In both cells, three sets of crystallographic orientations are considered: $x[100]$-$y[010]$-$z[001]$, $x[1\bar{1}1]$-$y[1\bar{1}\bar{2}]$-$z[110]$, and $x[1\bar{1}0]$-$y[11\bar{2}]$-$z[111]$, referred to as ⟨100⟩-, ⟨110⟩-, and ⟨111⟩-oriented models, respectively. In the bulk single crystal, a cube is employed, with periodic boundary conditions (PBCs) applied along all three directions. In the NTs, hollowed cylinders with a fixed height and varying outer radius R and wall thickness t are studied. PBCs are applied along the axial z direction, while the lateral surfaces are assumed traction-free. In particular, we study $R = 5$, 10, 15, or 20 nm, while t is varied accordingly. Note that when $t = R$, the models effectively represent NWs, which contain up to 4 218 852 atoms. The simulation cell sizes of the bulk single crystals and NWs/NTs are summarized in Table I.

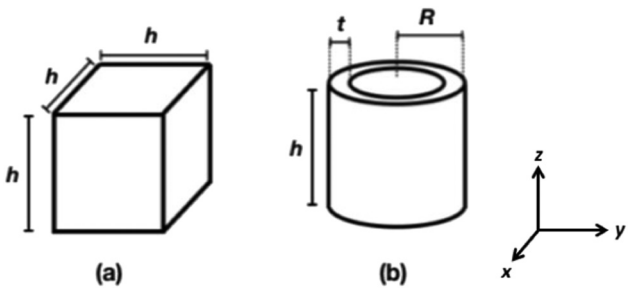

FIG. 1. Simulation cells of (a) the bulk single crystals and (b) the NTs. In (a), h is the edge length of the cube; in (b), R, t, and h are the outer radius, wall thickness, and cylinder height, respectively. In both models, the tensile deformation is applied along the z direction, which is along ⟨100⟩, ⟨110⟩, or ⟨111⟩ crystallographic orientation.

All MD simulations here are carried out using LAMMPS.[25] We use an embedded-atom method potential[26] known to well describe the generalized stacking fault energies, which are important for plastic deformation mechanisms including dislocation slip and twinning.[27–30] The lattice parameter is 3.143 39 Å. In all simulations, an NPT ensemble and an NVT ensemble are applied, respectively, to the bulk single crystals and the NTs/NWs, with a constant time step size of 2 fs at 300 K. Each model initially undergoes a dynamic relaxation for 250 ps, followed by tensile deformation along the z direction with a constant engineering strain rate $\dot{\varepsilon} = 10^8\ \mathrm{s}^{-1}$. Note that for bulk single crystals, the stress tensor components associated with the x and y directions are zeroed during the uniaxial deformation via the NPT ensemble. All atomic structures are visualized by OVITO,[31] while the defects (e.g., dislocations) are identified by the centrosymmetry parameter (CSP).[32]

III. RESULTS

A. Deformation mechanisms

For reference, the deformation behavior of bulk W single crystals is studied under the same loading condition as we will use for the NWs and NTs. After dynamic relaxation, no lattice defects exist in the bulk single crystals. During the subsequent tensile

TABLE I. Edge lengths of the bulk single crystals and NWs/NTs with the tensile deformation applied along ⟨100⟩, ⟨110⟩, or ⟨111⟩ direction. R varies from 5, 10, 15, to 20 nm.

Model	Tensile direction	L_x (nm)	L_y (nm)	L_z (nm)
Bulk	$z\langle 100\rangle$	50.29	50.29	50.29
	$z\langle 110\rangle$	49	50.05	48.9
	$z\langle 111\rangle$	50.05	48.9	49
NW/NT	$z\langle 100\rangle$	$2R$	$2R$	50.29
	$z\langle 110\rangle$	$2R$	$2R$	48.9
	$z\langle 111\rangle$	$2R$	$2R$	49

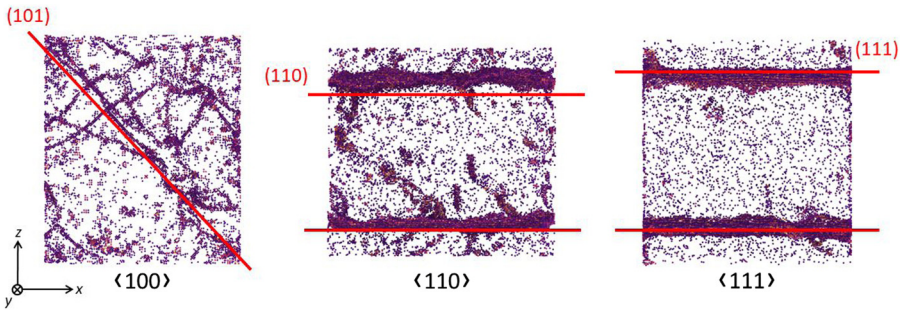

FIG. 2. Atomistic structures of the bulk single crystals taken when: the first dislocations are nucleated for the ⟨100⟩ orientation, and the first cracks are formed for ⟨110⟩ and ⟨111⟩ orientations. All atoms with a CSP smaller than 1.5 are removed and the remaining atoms are colored by CSP.

TABLE II. Schmid factors m for the slip planes {110} in all W models with the tensile deformation applied along ⟨100⟩, ⟨110⟩, or ⟨111⟩ direction. It is found that dislocations are most likely to form in ⟨100⟩-oriented models and least in ⟨111⟩-oriented models.

Slip plane	Slip direction	$m_{\langle 100\rangle}$	$m_{\langle 110\rangle}$	$m_{\langle 111\rangle}$
(110)	$[\bar{1}11]$	0.4082	0	0.2722
	$[1\bar{1}1]$	0.4082	0	0.2722
$(1\bar{1}0)$	[111]	0.4082	0	0
	$[\bar{1}\bar{1}1]$	0.4082	0	0
(011)	$[1\bar{1}1]$	0	0	0.2722
	$[\bar{1}\bar{1}1]$	0	0.4082	0.2722
$(0\bar{1}1)$	[111]	0	0.4082	0
	$[\bar{1}11]$	0	0	0
(101)	$[\bar{1}11]$	0.4082	0	0.2722
	$[\bar{1}\bar{1}1]$	0.4082	0.4082	0.2722
$(\bar{1}01)$	[111]	0.4082	0.4082	0
	$[1\bar{1}1]$	0.4082	0	0

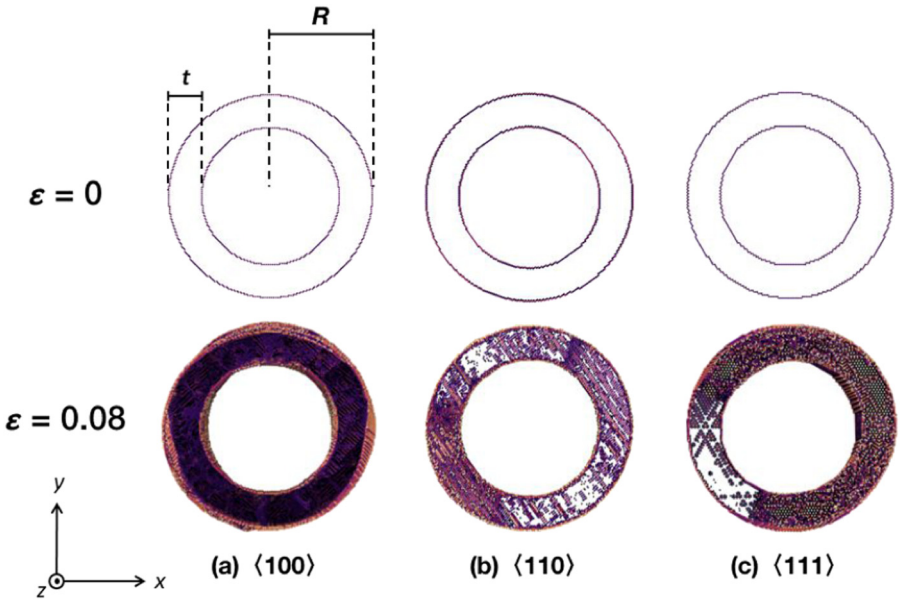

FIG. 3. Atomistic structures of the NTs with $R = 15$ nm and $t = 5$ nm. The first row is taken at the end of dynamic relaxation before any deformation has occurred, while the second row is taken at strain $\varepsilon = 0.08$. All atoms with a CSP smaller than 1 are removed and the remaining atoms are colored by CSP.

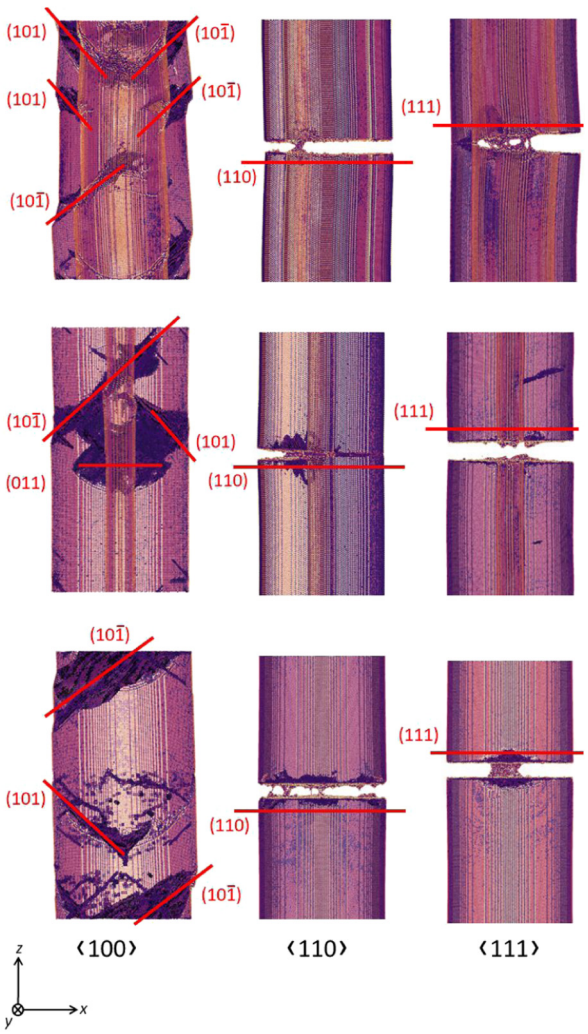

FIG. 4. Atomistic structures of the NTs and NWs with $R = 15$ nm taken when: in ductile failure, the first dislocations are nucleated for the ⟨100⟩ orientation; and, in brittle failure, the first cracks are formed for ⟨110⟩ and ⟨111⟩ orientations. (Top) $t = 4$ nm and $V{:}S = 1$ nm. (Middle) $t = 12$ nm and $V{:}S = 6$ nm. (Bottom) $t = 15$ nm (NW) and $V{:}S = 7.5$ nm. Slip and cleavage planes are marked by red lines. All atoms with a CSP smaller than 1 are removed and the remaining atoms are colored by CSP.

deformation, we observe that the failure mode of the bulk crystal, i.e., ductile vs brittle, depends on the crystallographic orientation. Here, the failure mode is identified based on the analysis of the atomistic structures at failure. If the dislocation slip is observed without crack formation, the deformation is considered ductile. If cracks are formed in the absence of dislocation slip, the deformation is considered brittle. The ⟨100⟩-oriented bulk single crystal fails in a ductile manner with dislocations nucleating on multiple {110} glide planes. In contrast, the ⟨110⟩- and ⟨111⟩-oriented crystals fail in a brittle manner by the formation of cracks on the {110} and {111} planes, respectively, as shown in Fig. 2. In general, BCC crystals could also deform via glide on the {112} planes; however, in the W single crystals, we observe no dislocation activation of the {112} slip mode under tension in any of these three single crystals. Table II presents the Schmid factors for all 12 slip systems belonging to the {110} slip mode. Consistent with the ductile-to-brittle orientation dependence seen in simulations, ⟨100⟩-oriented loading projects nearly ideal amounts of shear (i.e., factors close to 0.5) in eight slip systems, whereas the other two orientations projects shear in less amounts and/or fewer systems.

Next, to study the effects of nanostructuring and size, the deformation mechanisms and failure modes of NTs and NWs are studied. The first row of Fig. 3 shows that the morphology of the NTs and NWs remains unchanged after dynamic relaxation. As in the bulk single crystals, no defects exist in the undeformed NTs/NWs. This result is seen for all orientations and agrees with a prior study of ⟨112⟩-oriented NTs in W.[15] This atomically smooth surface morphology, however, is different from Au NTs whose free surfaces are reconstructed to the more energetically favorable {111} facets after dynamic relaxation.[7] We further remark that the free surface reconstruction occurs only in Au NTs but not in Au NWs.[33]

When subject to tensile deformation, the NWs exhibit either ductile or brittle behavior. In NTs, however, the identification of ductile or brittle modes may not be definite because sometimes it is difficult to distinguish between dislocations and other lattice defects close to or attached to the free surfaces. When this occurs, we consider the deformation as "semiductile." The second row of Fig. 3 shows snapshots of the atomistic structures in NTs at strain $\varepsilon = 0.08$. Similar to the anisotropic responses for the bulk single crystals, NTs and NWs with the same outer radius R and wall thickness t tend to be ductile when they are ⟨100⟩-oriented and brittle when they are ⟨111⟩-oriented. As shown in Fig. 4, in the ductile mode, dislocations on the (011), (101), and (10$\bar{1}$) planes

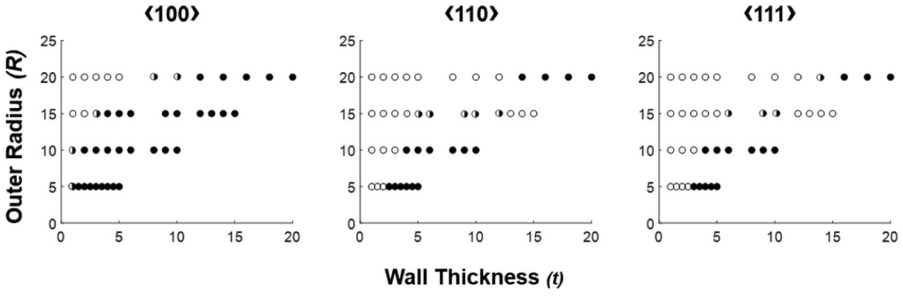

FIG. 5. Map indicating whether each NT or NW failed in a ductile (filled circles), semiductile (half-filled circles), or brittle (open circles) manner.

nucleate from the inner or outer surfaces; in the brittle mode, cracks are formed without the dislocation slip. No deformation twins formed for any NT or NW geometry.

However, unlike the bulk crystals, for the same orientation, whether a specific NT or NW fails in a ductile or brittle manner also depends on R and t. This dependency is summarized in Fig. 5. For the same R, NTs with a thinner wall ($t = 1$ nm) are more brittle, while those with a thicker wall, which are more like NWs, tend to be more ductile. For the same t, however, no clear trend regarding how R influences the brittle/ductile mode emerges.

B. Stress-strain response

Figure 6 presents the stress-strain curves of NTs and NWs with $R = 5$ nm. Curves for the other values of R are similar and not shown in the interest of space. In these calculations, the engineering stress is calculated through the summation of the virial stress of all atoms. Along each stress-strain curve, the maximum stress is taken as the ultimate stress σ_U. The critical stress and strain corresponding to the point after which the stress-strain relation is no longer linear are considered the yield stress σ_Y and yield strain ε_Y, respectively. Accordingly, Young's modulus $E = \sigma_Y/\varepsilon_Y$. Mechanical quantities for the NWs are denoted by superscript *. To help elucidate the role of NT geometry, we also consider the volume-to-surface-area ratio V:S for each NT, which is related to R and t via

$$V{:}S = \frac{\pi h(R^2 - r^2)}{2\pi h(R + r)} = \frac{(R + r)(R - r)}{2(R + r)} = \frac{t}{2}. \quad (1)$$

We note that the surface areas of the two bases are not included due to the application of PBCs along the axial z direction.

We first study Young's modulus E and its orientation dependence. For bulk W single crystals, E = 401, 407, and 411 GPa for ⟨100⟩, ⟨110⟩, and ⟨111⟩ lattice orientations, respectively. These values are close to the experimentally measured Young's modulus

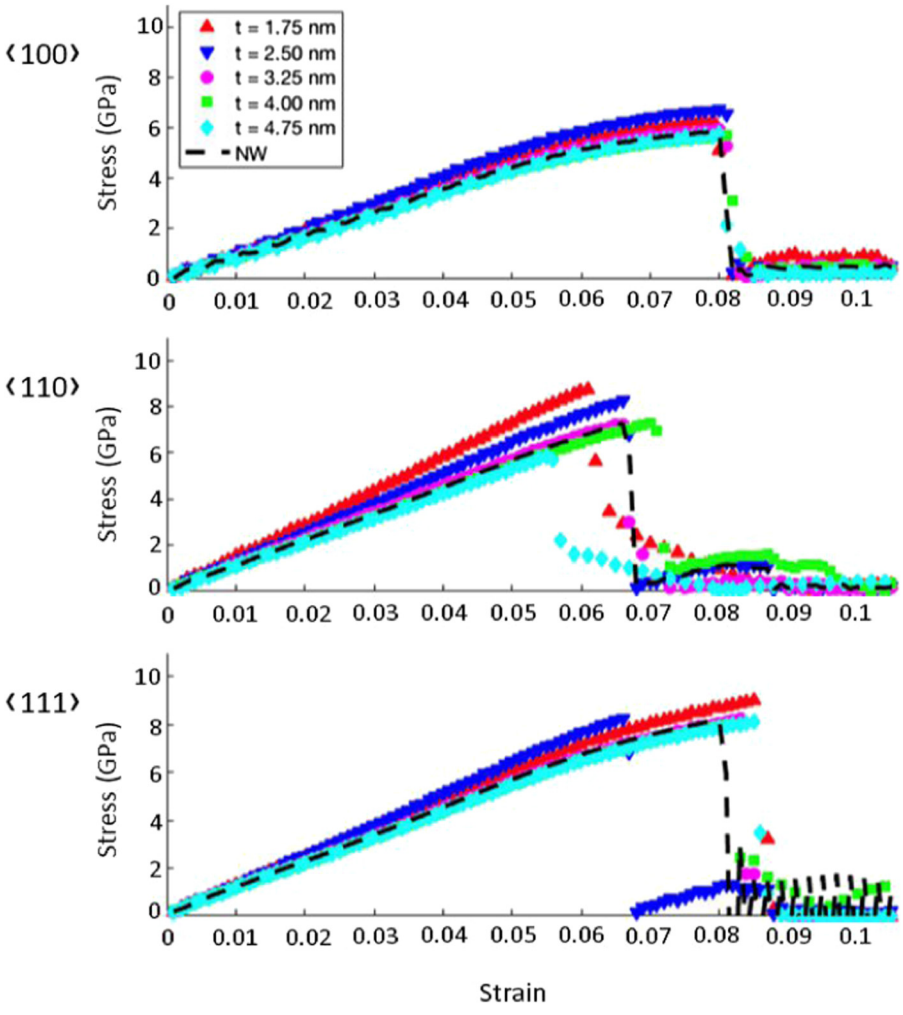

FIG. 6. Stress-strain curves for ⟨100⟩-, ⟨110⟩-, and ⟨111⟩-oriented NTs with $R = 5$ nm and various t. Results of NWs with the same R are also presented.

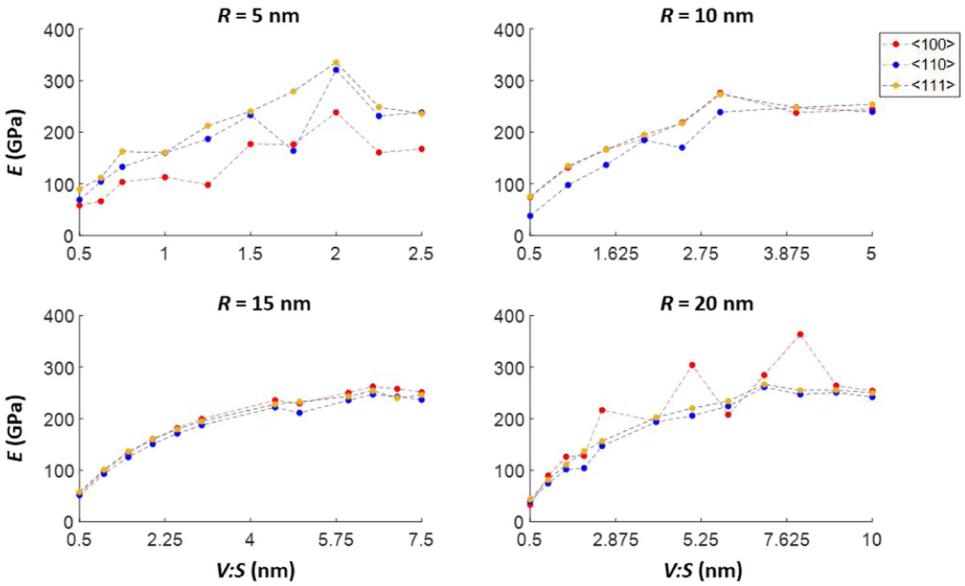

FIG. 7. Young's modulus E with respect to the volume-to-surface-area ratio V:S for NTs/NWs with various outer radii R. For each R, the rightmost point represents the NW with $V{:}S = t/2 = R/2$.

of W polycrystals (411 GPa)[34] and the small orientation sensitivity is consistent with the low elastic anisotropy index measured for W.[35] One reason for choosing W in this study was the possibility of minimizing any effects of elastic anisotropy in the analysis of NT size effects on strengths and ductile-to-brittle transitions.

The calculated Young's moduli of the NTs and NWs are given in Fig. 7. For the same NT geometry, i.e., R and V:S, the difference in E between differently oriented NTs is smaller for a larger R or a larger V:S (i.e., a thicker wall). On the one hand, E is isotropic in bulk single crystals, so the anisotropic E is attributed to the atomic bonding on the free surfaces. On the other hand, NTs with a larger R or V:S have a higher proportion of surface atoms, whose configurations vary with the axial crystallographic orientation.

Unlike bulk crystals and NWs, NTs bear an additional geometric parameter, the wall thickness t, which can affect E. Figure 7 shows the change in E with V:S ($=t/2$), where the rightmost data point in each plot corresponds to E of the NW with the same R. Overall, we observe that the NTs and NWs are not as stiff as the bulk crystal and NTs are not as stiff as NWs. The tensile stiffness of NTs and NWs can be increased to that of the buik value by

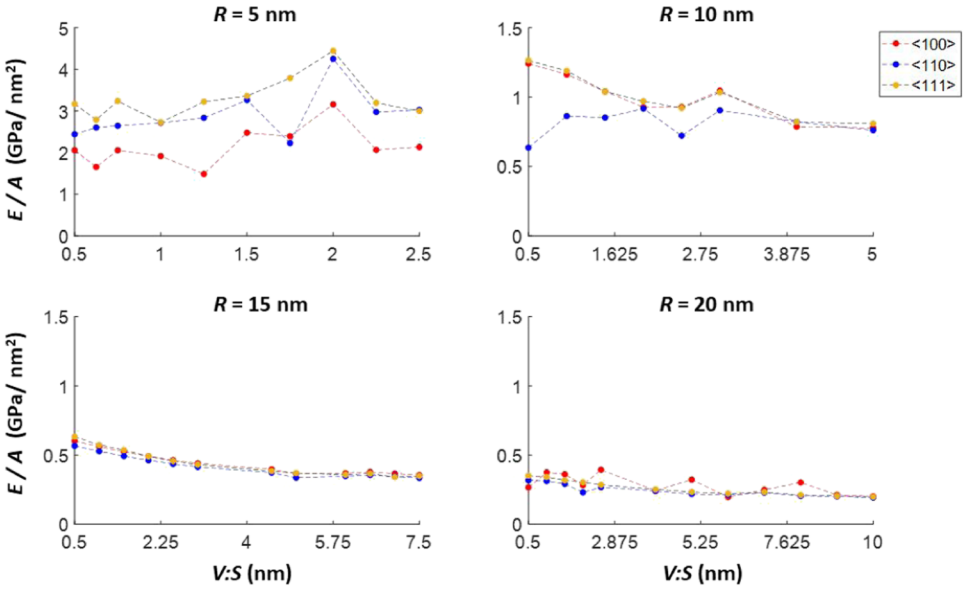

FIG. 8. The specific Young's modulus E/A, where A is the cross-sectional area, with respect to the volume-to-surface-area ratio V:S for NTs/NWs with various outer radii R. For each R, the rightmost point represents the NW with $V{:}S = t/2 = R/2$.

increasing the outer radius R. For NTs, reductions in E relative to the NW with the same R can be attained by making the NT thinner. Therefore, the NT wall thickness t provides a way to further adjust the compliance of the structure.

For lightweight structures, like trusses and foams, the specific Young's modulus E/A, Young's modulus divided by the cross-sectional area of the NT or NW, is of arguably greater importance than E. In this light, NTs and NWs can be superior to their bulk counterparts. Figure 8 shows the variation in the specific tensile stiffness of the NTs with respect to NT geometry. From these results, we find that the most effective way to increase the specific tensile stiffness of NTs and NWs is to decrease R. For both NTs and NWs alike, higher specific moduli can be achieved as R decreases. As shown in Fig. 8, the variation in specific modulus with V:S for a given R is small. As V:S decreases (i.e., thinner t), NTs slightly outperform NWs in specific elasticity. It is worth remarking that other crystals of high cubic symmetry in structure, such as FCC Ni, have reported similar trends.[13]

Next, we focus on the effect of NT geometry on ultimate stress σ_U and yield stress σ_Y. These properties as we have seen earlier are mediated either by crystallographic slip or cracking. While it is found here that NTs do not provide significantly higher stiffness than NWs, the results here show that NTs can provide noticeably higher strengths than NWs for the same R. Figure 9 shows the variation in the calculated σ_U and σ_Y normalized by their corresponding NW values σ_U^* and σ_Y^*, with respect to V:S. In nearly all cases studied, the yield and ultimate strengths of the NTs exceed those of the NWs with the same R. NT strengths can rise further above NW strengths as R increases and t decreases. Exceptions are the $R = 5$ nm case with larger V:S and the $R = 20$ nm case for the ⟨110⟩-oriented NTs. It is worth remarking that these anomalies have no relation to the failure mode. Some of these weaker NTs failed in a brittle manner and some in a ductile manner. We note that, according to Table II, the ⟨110⟩-oriented system is unique in that it is more likely to simultaneously activate slip in two directions on different planes, in contrast to the other two load orientations. Since the NTs have two surfaces from which dislocations can nucleate, instead of one surface in NWs, it is more likely in the ⟨110⟩-oriented NTs that dislocations on different crstallographic slip planes intersect with each other as the volume increases. This may explain why the NTs have a lower yield and ultimate strength than the NWs for the ⟨110⟩ orientation only when the volume is the largest studied, $R = 20$ nm.

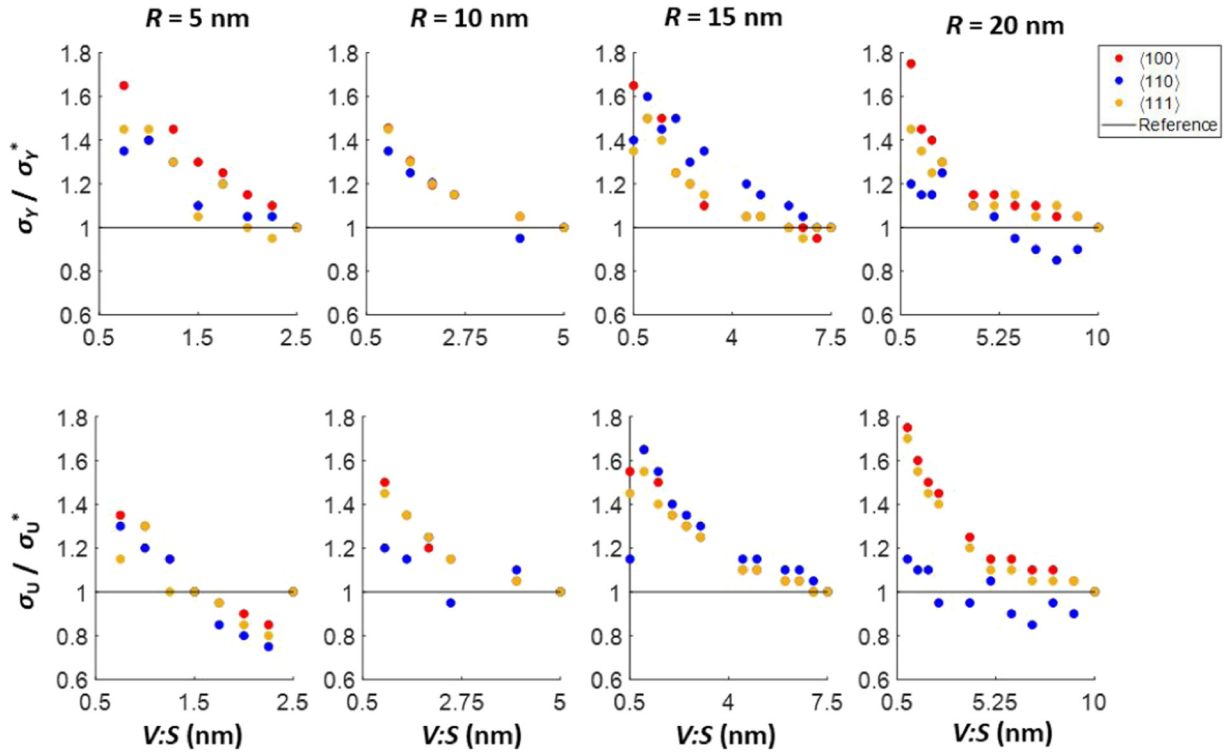

FIG. 9. The yield stresses σ_U and ultimate stresses σ_Y of NTs are, respectively, normalized by the corresponding NW values σ_U^* and σ_Y^*. The normalized values are plotted against the volume-to-surface-area ratio V:S to show the effects of the latter on the strengthening of NTs over NWs. For each outer radius R, the rightmost point represents the NW with V:$S = R/2$.

IV. DISCUSSION

In this work, we examine the effects of NT geometry, specifically the outer radius R and wall thickness t on elastic and plastic deformation response and failure mode. To determine whether NT geometry heightens orientation sensitivity in an otherwise nearly isotropic material, we tested different crystallographic orientations. Unlike the bulk crystal, the elastic response of the NTs is not isotropic. For example, NT geometry can adjust the tensile stiffness E. We find here that for NTs with the same outer radius R, E will reduce or the NT become more compliant, as t decreases. The stiffness E of the NW serves as a practical upper bound to the tensile specific stiffness of the NT with the same R. Although NTs may not offer higher stiffness than NWs, they do allow for the opportunity to tune the stiffness. Slight increases in specific stiffness E/A are possible with NTs, especially as t decreases. Combined with the strength gains associated with NT with finer t, the implication is that NTs can provide a geometry with much higher strength-to-weight ratios than NWs with the same R.

The crystallographic orientation has a profound influence on the failure mode. Our analysis reveals that NWs bear the same dependency of failure mode on the orientation as bulk crystals. However, by tuning the wall thickness t, NTs offer a way to change the failure mode from brittle to ductile. The effectiveness of the NT "ductilizing" effect depends on orientation. For the ⟨100⟩ orientation, the bulk crystals and NWs are ductile, and the NTs for most geometries are also ductile. This is consistent with MD simulations of W in the ⟨112⟩-orientation, wherein bulk crystals, NWs ($5\ \text{nm} \leq R \leq 70\ \text{nm}$), and NTs ($R = 20\ \text{nm},\ t > 2\ \text{nm}$) of this orientation failed in a ductile manner. For both ⟨110⟩- and ⟨111⟩-oriented structures, the bulk crystals and NWs are brittle, but remarkably a large number of NTs failed in a ductile mode. In particular, the NT geometry is the most effective in ductilizing the material for the ⟨110⟩ orientation. Taken together, these calculations imply that altering the structure of a NW to a NT can not only increase strength, strength-to-weight but also render a normally brittle material ductile.

It is useful to compare our MD simulation results with those based on experiments. To the best of our knowledge, there is only one *in situ* transmission electron microscope (TEM) experimental work in the literature[36] concerning tensile deformation of W NWs with axial orientations of ⟨100⟩, ⟨110⟩, and ⟨111⟩. In Ref. 36, $R \approx 15\ \text{nm}$ and W NWs with all three orientations failed in a ductile mode. However, the plastic deformation was dominated by twinning instead of the dislocation slip observed in our simulations. Note that there exist quantitative differences between the TEM experiments and the current MD simulations. The NWs in experiments were bicrystals, while those in MD simulations are single crystals. The strain rate in experiments ($10^{-3}\ \text{s}^{-1}$) was much lower than that in MD simulations ($10^{8}\ \text{s}^{-1}$).

V. CONCLUSIONS

In this work, atomistic simulations are performed to analyze the tensile deformation of NTs in BCC W, with an emphasis on how the deformation mechanisms and mechanical properties change with the crystallographic orientation along the axial z direction, the wall thickness t, and the outer radius R. Bulk single crystals and NWs are also investigated subject to the same loading for references. Results are summarized as follows:

(1) After dynamic relaxation, the morphology of NWs remains unchanged, similar to Au NWs. However, different from Au NTs whose surfaces undergo reconstruction during dynamic relaxation, the morphology of the W NTs still remains unchanged.
(2) The elastic and plastic response of NTs and NWs exhibits some anisotropy, unlike bulk crystalline W. The NT z-orientation affects greatly the brittle vs ductile failure mode.
(3) Subject to the tensile loading, ⟨100⟩-oriented bulk single crystals fail in a ductile manner, while the ⟨110⟩- and ⟨111⟩-oriented ones fail in a brittle manner. The same trend is observed in NWs, where ductile NWs exhibited slip-dominated deformation and nucleation of dislocations from the surface.
(4) Significantly, the mode of failure of NTs, for the same z-orientation, whether ductile or brittle, depends on t and R. For the three orientations considered in this work, we found that NTs with a thinner wall tend to be more brittle.
(5) For NTs, compared with the NW with the same R, E decreases with a smaller t. While Young's modulus E of the NTs and NWs are much smaller than that of the bulk single crystals, the specific modulus of the NT can be made higher than that of a NW with the same R with a thinner wall.
(6) In addition, both ultimate stress and yield stress vary more significantly with t than with R. Still, NTs, on average, outperform NWs with the same R in both ultimate and yield strengths.

ACKNOWLEDGMENTS

The authors gratefully acknowledge support from the Office of Naval Research (ONR) under contract ONR BRC Grant No. N00014-18-1-2392. The work of S.X. was supported in part by the Elings Prize Fellowship in Science offered by the California NanoSystems Institute on the UC Santa Barbara campus. Use was made of computational facilities purchased with funds from the National Science Foundation (NSF) (No. CNS-1725797) and administered by the Center for Scientific Computing (CSC). The CSC is supported by the California NanoSystems Institute and the Materials Research Science and Engineering Center (MRSEC; NSF DMR No. 1720256) at UC Santa Barbara. This work used the Extreme Science and Engineering Discovery Environment (XSEDE), which is supported by the National Science Foundation (Grant No. ACI-1053575).

REFERENCES

[1]G. L. Hornyak, J. J. Moore, H. Tibbals, and J. Dutta, *Fundamentals of Nanotechnology* (CRC Press, 2009).
[2]N. G. Portney and M. Ozkan, Anal. Bioanal. Chem. **384**, 620 (2006).
[3]S. Xu, M. I. Latypov, and Y. Su, Philos. Mag. Lett. **98**, 173 (2018).
[4]R. Maaß, V. Van Petegem, D. Ma, J. Zimmermann, D. Grolimund, F. Roters, H. Van Swygenhoven, and D. Raabe, Acta Mater. **57**, 5996 (2009).
[5]X. Li and H. Gao, Nat. Mater. **15**, 373 (2016).
[6]B. Wu, A. Heidelberg, and J. J. Boland, Nat. Mater. **4**, 525 (2005).
[7]R. Cao, Y. Deng, and C. Deng, Acta Mater. **86**, 15 (2015).
[8]J. R. Greer and W. D. Nix, Phys. Rev. B **73**, 245410 (2006).
[9]M. Sun, F. Xiao, and C. Deng, Appl. Phys. Lett. **103**, 231911 (2013).
[10]E. P. M. Amorim, A. J. R. da Silva, and E. Z. da Silva, J. Phys. Chem. C **112**, 15241 (2008).

[11]C. Ji and H. S. Park, Appl. Phys. Lett. **89**, 181916 (2006).
[12]C. Ji and H. S. Park, Nanotechnology **18**, 115707 (2007).
[13]L. Wang, C. Peng, and J. Gong, Euro. J. Mech. A **28**, 877 (2009).
[14]J. Rojas-Nunez, F. Valencia, R. I. Gonzalez, E. M. Bringa, S. Allende, J. L. Palma, A. Pereira, J. Escrig, and S. E. Baltazar, Comput. Mater. Sci. **168**, 81 (2019).
[15]S. Xu and S. Z. Chavoshi, Curr. Appl. Phys. **18**, 114 (2018).
[16]C. Weinberger, B. Boyce, and C. Battaile, Int. Mater. Rev. **58**, 296 (2013).
[17]S. Xu, J. K. Startt, T. G. Payne, C. S. Deo, and D. L. McDowell, J. Appl. Phys. **121**, 175101 (2017).
[18]S. Xu, Y. Su, D. Chen, and L. Li, Appl. Phys. A **123**, 788 (2017).
[19]S. Xu, Int. J. Multiscale Comput. Eng. **16**, 367 (2018).
[20]D. Jang, X. Li, H. Gao, and J. R. Greer, Nat. Nanotechnol. **7**, 594 (2012).
[21]J. Wang, F. Sansoz, J. Huang, Y. Liu, S. Sun, Z. Zhang, and S. X. Mao, Nat. Commun. **4**, 1742 (2013).
[22]G. Sainath and B. K. Choudhary, Philos. Mag. **96**, 3502 (2016).
[23]S. Xu, S. Z. Chavoshi, and Y. Su, Phys. Status Solidi RRL **12**, 1700399 (2018).
[24]Z. Z. Fang, X. Wang, T. Ryu, K. S. Hwang, and H. Sohn, Int. J. Refra. Metal. Hard Mater. **27**, 288 (2009).
[25]S. Plimpton, J. Comput. Phys. **117**, 1 (1995).
[26]M.-C. Marinica, L. Ventelon, M. R. Gilbert, L. Proville, S. L. Dudarev, J. Marian, G. Bencteux, and F. Willaime, J. Phys. Condens. Matter **25**, 395502 (2013).
[27]S. Xu, L. Xiong, Y. Chen, and D. L. McDowell, JOM **69**, 814 (2017).
[28]S. Z. Chavoshi, S. Xu, and S. Goel, Proc. R. Soc. A **473**, 20170084 (2017).
[29]S. Xu and Y. Su, Phys. Lett. A **382**, 1185 (2018).
[30]S. Xu, Y. Su, and S. Z. Chavoshi, Mater. Res. Express **5**, 016523 (2018).
[31]A. Stukowski, Modell. Simul. Mater. Sci. Eng. **18**, 015012 (2010).
[32]C. L. Kelchner, S. J. Plimpton, and J. C. Hamilton, Phys. Rev. B **58**, 11085 (1998).
[33]S. Lee, J. Im, Y. Yoo, E. Bitzek, D. Kiener, G. Richter, B. Kim, and S. H. Oh, Nat. Commun. **5**, 3033 (2014).
[34]E. Lassner and W.-D. Schuber, *Tungsten: Properties, Chemistry, Technology of the Element, Alloys, and Chemical Compounds* (Kluwer Academic, 1998).
[35]S. I. Ranganathan and M. Ostoja-Starzewski, Phys. Rev. Lett. **101**, 055504 (2008).
[36]J. Wang, Z. Zeng, C. R. Weinberger, Z. Zhang, T. Zhu, and S. X. Mao, Nat. Mater. **14**, 594 (2015).